REPORT DOCUMENTATION PAGE

Form Approved
OMB No. 0704-0188

1. REPORT DATE (DD-MM-YYYY)	2. REPORT TYPE	3. DATES COVERED (From - To)
31/07/02	FINAL TECHNICAL	2/1/99 - 11/30/01

4. TITLE AND SUBTITLE
Corrosion-Induced Multiple Site Damage

5a. CONTRACT NUMBER

5b. GRANT NUMBER
F49620-99-1-0136

5c. PROGRAM ELEMENT NUMBER

6. AUTHOR(S)
Karl Sieradzki
Dusan Krajcinovic

5d. PROJECT NUMBER

5e. TASK NUMBER

5f. WORK UNIT NUMBER

7. PERFORMING ORGANIZATION NAME(S) AND ADDRESS(ES)
Arizona State University
Dept. of Mechanical and
Aerospace Engineering
Tempe, Arizona 85287-6106

8. PERFORMING ORGANIZATION REPORT NUMBER
XAA 0060/TE

9. SPONSORING / MONITORING AGENCY NAME(S) AND ADDRESS(ES)
Air Force Office of Scientific Research, AFOSR/NA
Walter F. Jones
801 North Randolph Street
Room 732
Arlington, VA 22203-1977

10. SPONSOR/MONITOR'S ACRONYM(S)
AFOSR

11. SPONSOR/MONITOR'S REPORT NUMBER(S)

12. DISTRIBUTION / AVAILABILITY STATEMENT
Unlimited

20020815 092

13. SUPPLEMENTARY NOTES

14. ABSTRACT

This research focuses on three key issues related to the nucleation and growth of corrosion fatigue cracks in fuselage fastener holes. (1) The identification of the precise mechanisms responsible for corrosion damage in Al alloy 2024-T3 in the bare, clad, and painted condition. (2) The transitional behavior from corrosion damage to fatigue crack growth nucleation and subsequent short crack growth, and (3) a real-time statistically based model of damage evolution in a structural element.

Another aspect of the multiple site damage (MSD) problem that we address is related to the striking observation that that there is relative size uniformity of the fatigue cracks from rivet to rivet. The transition from uniform damage (mean field behavior) to that dominated by the propagation of the largest crack in the system is a key aspect of lap joint failure. Often, the onset of such a transition is determined by monitoring the changes occurring in a suitable *order parameter*. Several possible scenarios for this behavior are explored including chemical short crack effects, and local load redistribution processes similar to what occurs during damage evolution in parallel bar models.

15. SUBJECT TERMS
Corrosion fatigue, Multiple site damage, order parameter, parallel bar model

16. SECURITY CLASSIFICATION OF:			17. LIMITATION OF ABSTRACT	18. NUMBER OF PAGES	19a. NAME OF RESPONSIBLE PERSON
a. REPORT	b. ABSTRACT	c. THIS PAGE		11	Karl Sieradzki
					19b. TELEPHONE NUMBER (include area code) (480) 965-8990

Corrosion-Induced Multiple Site Damage

THE FOLLOWING WAS ORIGINALLY SUBMITTED IN SEPTEMBER 2001 AND WAS MEANT TO SERVE AS A FINAL REPORT

AFOSR Aging Aircraft Final Program Report 2001

K. Sieradzki* and D. Krajcinovic
Department of Mechanical and Aerospace Engineering
Arizona State University
Tempe, Arizona 85287-6106

*K. Sieradzki, tel: 480-965-9100, fax: 480-965-1384, email: karl@icarus.eas.asu.edu

1. Executive Summary (Introduction)

Herein we describe research done over the past year on our AFOSR program, "Corrosion-Induced Multiple Site Damage". This research focuses on three key issues related to the nucleation and growth of corrosion fatigue cracks in fuselage fastener holes. (1) The identification of the precise mechanisms responsible for corrosion damage in Al alloy 2024-T3 in the bare, clad, and painted condition. (2) The transitional behavior from corrosion damage to fatigue crack growth nucleation and subsequent short crack growth, and (3) a real-time statistically based model of damage evolution in a structural element.

Another aspect of the multiple site damage (MSD) problem that we address is related to the striking observation that that there is relative size uniformity of the fatigue cracks from rivet to rivet. The transition from uniform damage (mean field behavior) to that dominated by the propagation of the largest crack in the system is a key aspect of lap joint failure. Often, the onset of such a transition is determined by monitoring the changes occurring in a suitable *order parameter*. We propose to explore several possible scenarios for this behavior including chemical short crack effects, and local load redistribution processes similar to what occurs during damage evolution in parallel bar models. As described in this report, the major results of our work over the past year are the following.

- statistical characterizations second phase particles in Al alloy 2024-T3 in order to identify the nature of incipient fatigue crack nuclei
- development of system and initiation of measurement of the kinetics of corrosion induced stress buildup from processes such as pillowing
- A modeling study of length scale independent statistical scaling of distributions associated with corrosion induced damage.

1.2 Graduate students supported by this program

Lei Tang (100%)
Ratsko Vasill (100%)

1.3 Major Accomplishments

We have completed what we believe to be the most comprehensive study to date measuring the statistics of corrosion damage on Al Alloy 2024-T3 in the RD, ST, and LT orientations as a function of time and sample size.

2.0 Modeling – Deformation induced by pillowing

In our analysis of pillowing stresses that evolve during experiments, it has become clear that there is no bending induced in the composite cantilever specimen. Consider the figure below showing the specimen used in experiments.

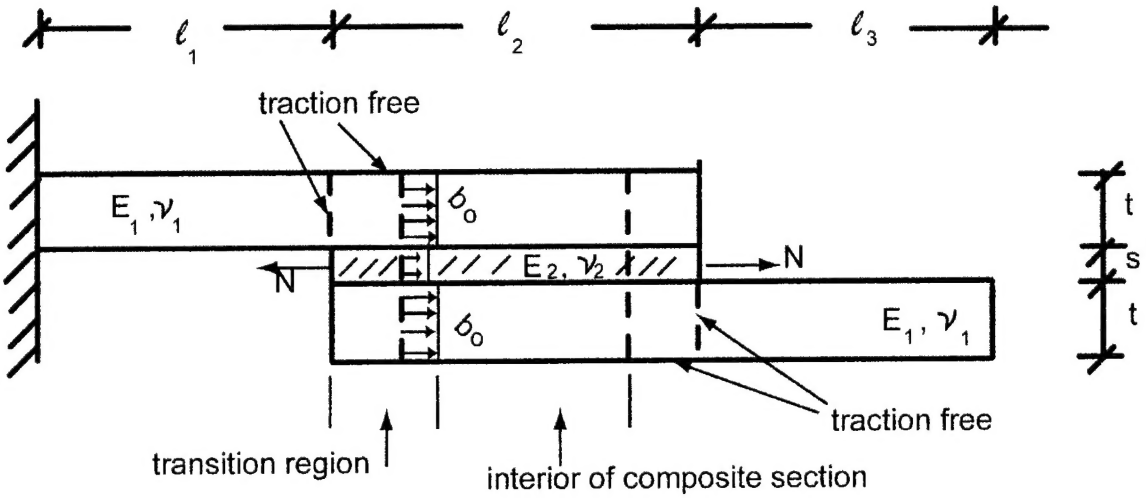

Here E_1 and ν_1 correspond to the Young's modulus and Poisson's ratio of the Al 2024-T3, E_2 and ν_2 are the corresponding quantities of the corrosion product which produces an eigenstrain, ε^*. The transformation strain, ε^* results from the corrosion product build-up and produces deformations indicated in the sketch below.

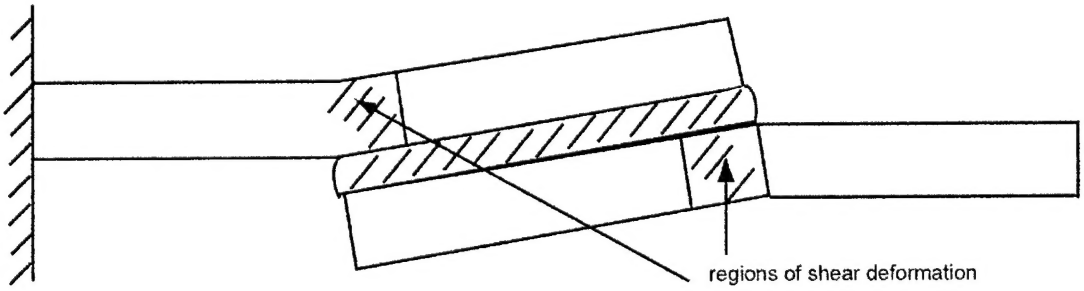

All of the deformation is localized to the shear regions indicated in the diagram above. A close-up of the shear deformation region on the left side of this figure is shown below.

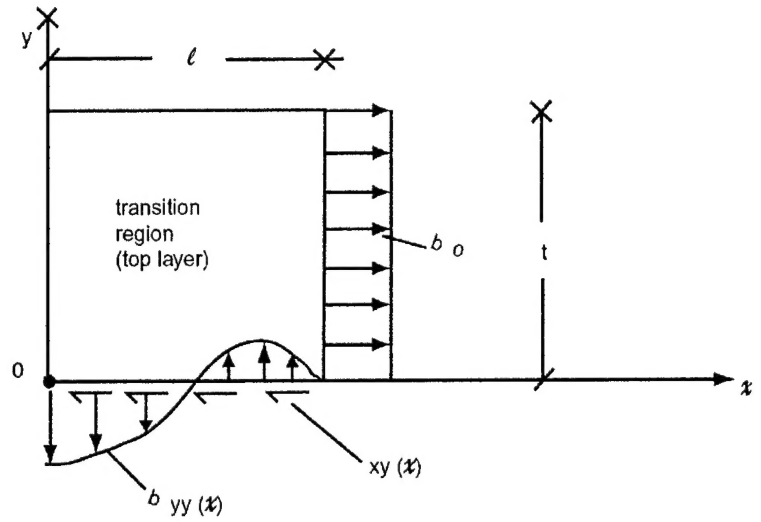

The transition region is subjected to 3 loading conditions:

(1) σ_o = constant on $x = l$, $0 \le y \le t$
(2) $\tau_{xy}(x)$ – the profile of which is unknown on $y = 0$, $0 \le x \le l$
(3) $\sigma_{yy}(x)$ - the profile of which is unknown on $y = 0$, $0 \le x \le l$

Consideration of static equilibrium leads to the following relations between these quantities.

$$\sum F_x = 0, \quad \int_0^l \tau_{xy}(x)dx = \sigma_o t, \text{ and}$$

$$\sum M_o = 0, \quad \int_0^l \sigma_{yy}(x)xdx = \frac{1}{2}\sigma_o t^2.$$

We can determine the combined effects of loading using linear superposition.

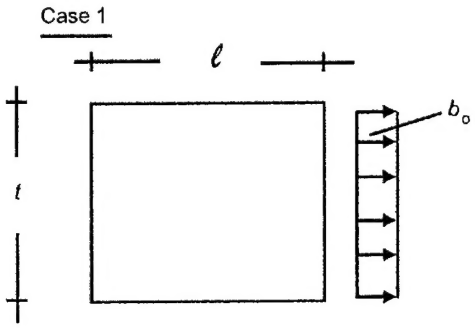

This case causes no rotation of the left wall, (i.e., $x = 0, \quad 0 \le y \le t$).

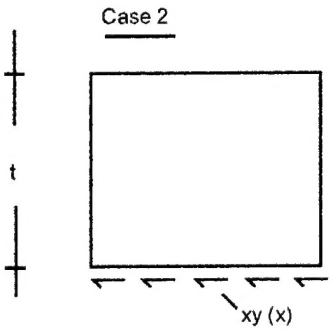

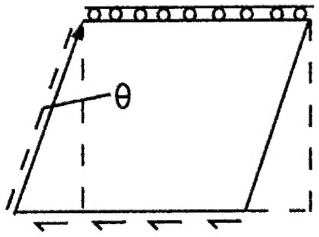

This will lead to distortion and the left vertical wall will rotate CW by an average angle θ.

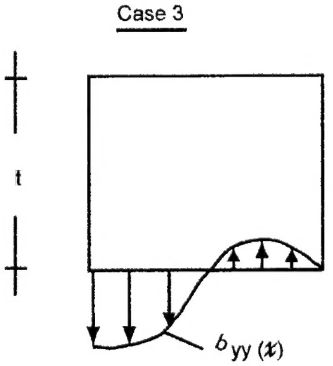

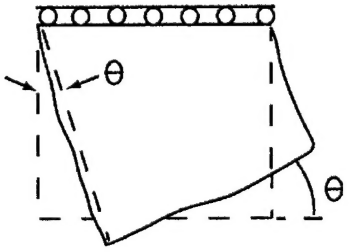

This causes rotation of the wall CCW by an average angle θ.

The angle θ can be estimated by detailed examination of case 2 or 3. In the shear loading case assuming the following linear form for $\tau_{xy}(x)$, $\tau_{xy}(x) = \frac{\tau_o}{t}(y - y)$, one can show that $\theta = \frac{\tau_o}{2G}$, where G is the shear modulus. Finally, the unknown quantity τ_o can be related to the transformation strain ε^*,

$$\theta = (1+\nu_1)\frac{t}{l}\frac{\varepsilon^*}{1+2\frac{t}{s}\frac{E_1}{E_2}\frac{1-\nu_2^2}{1-\nu_1^2}}.$$

The main aspects of this analysis have been confirmed with finite element methods. Measurement of the angle θ allows for the determination of the eigenstrain.

3.0 Statistics of pitting damage in Al alloy 2024-T3

Over the past year we have performed detailed statistical studies of corrosion induced pitting damage on Al alloy 20204-T3. RD and LT surfaces of Al alloy 2024-T3 were mechanically polished to a 0.05 μm finish in the and exposed to the following solutions, {concentrations indicated mM}:

- $Al(OH)_3$ {1.42}, $Ca(OH)_2$ {1.97}, $MgCl_2$ {0.11}, $MgSO_4$ {2.40}, $NaNO_3$ {0.108}, NaF {0.047}, resulting in a pH ~ 10.5 solution
- Cl^- {20}, NO^{2-} {4}, bicarbonate {4}, F^- {2} adjusted to pH 9.
- 0.5M Cl^-

Prior to and following exposure in an electrolyte for prescribed times, atomic force microscopy and high resolution scanning electron microscopy were used to characterize the size distribution of second phase particles and holes on the surface of the alloy. Exposure times of 0.5, 2.5, 6.0, 12, 31, 125, 200 and 318 hours were used for samples ranging in aerial size from $10^2 - 10^8$ μm^2. At least six samples of each size and exposure time are currently being examined.

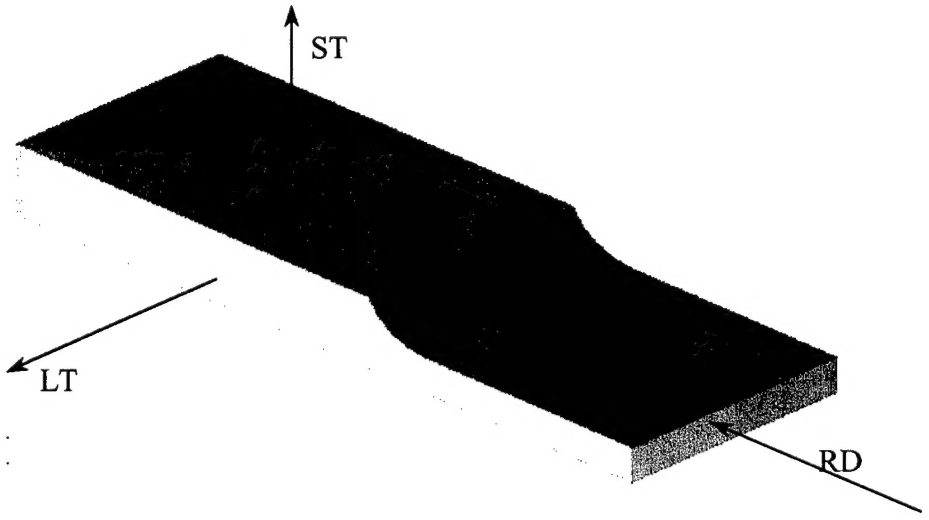

Fig. 1. The three surfaces studied surfaces on Al 2024-T3.

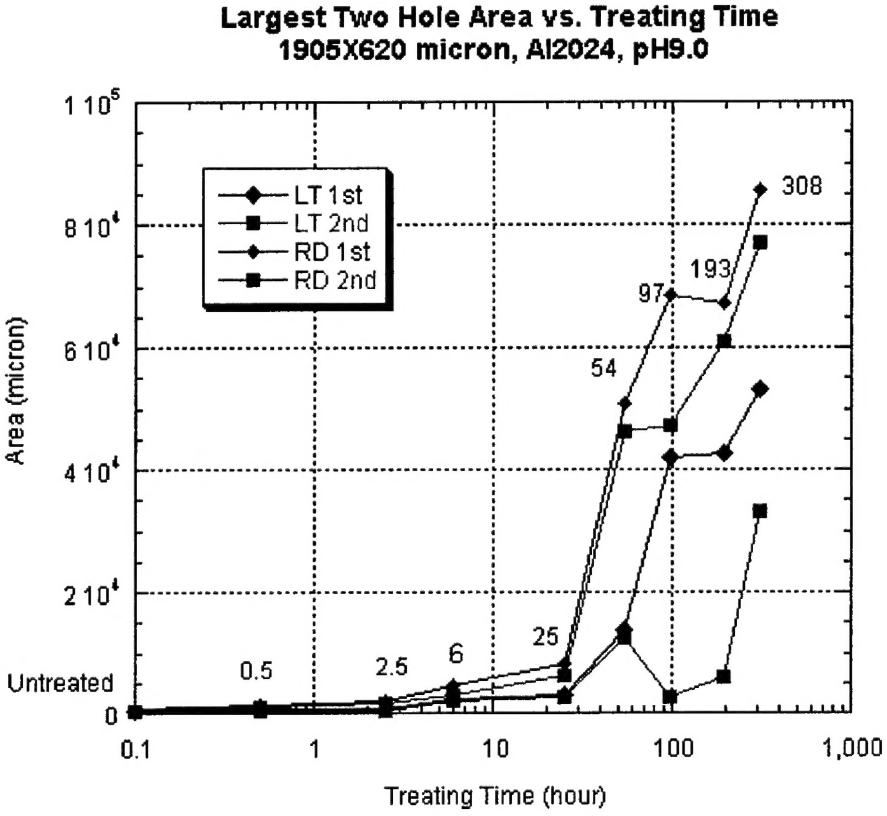

Fig.2. The first and second largest hole area of RD and LT surface vs. treating time with image size 1905X620.

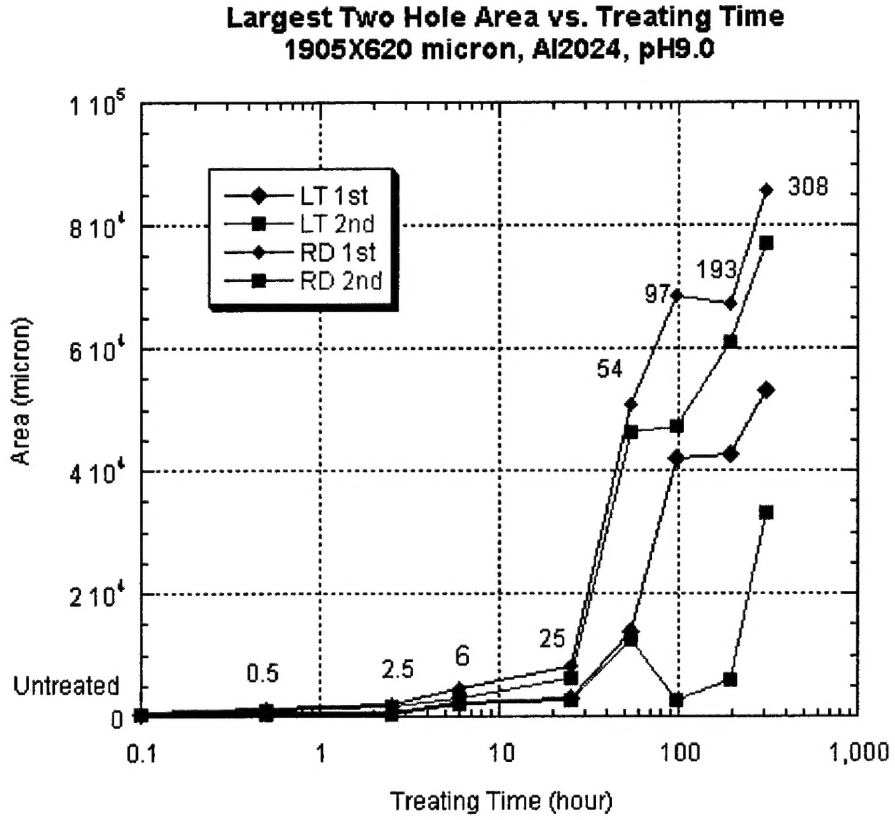

Fig.3. The first and second largest hole area of RD and LT surface vs. treating time with image size 1905X620.

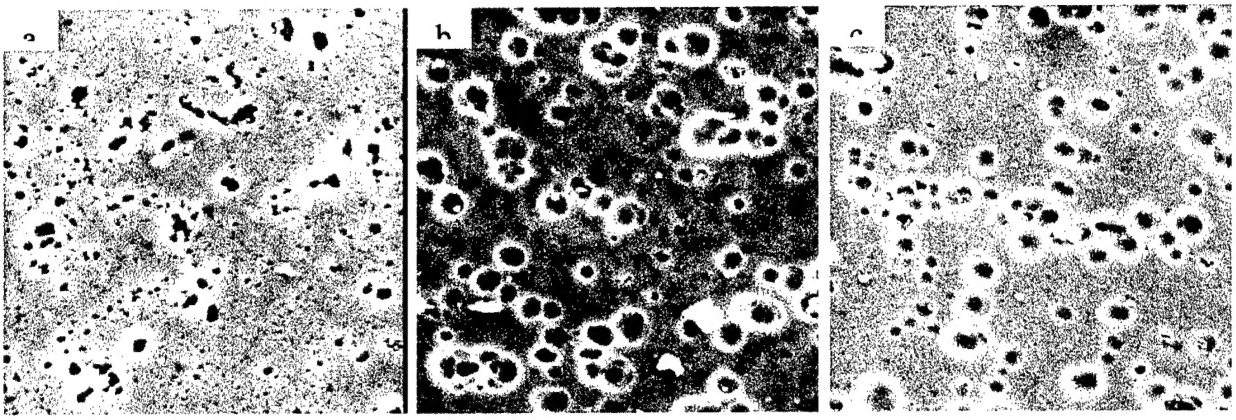

Fig. 4. The 108X108 (micron) SEM image for ST (a), LT (b) and RD (c) surface of Al2024 treated 308 hrs, pH9.0.

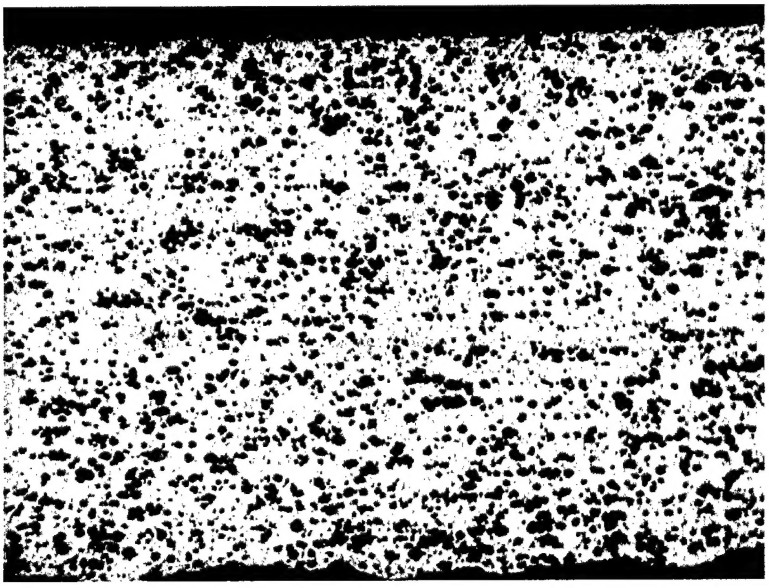

Fig. 5. The optical image of RD surface treated 308hrs. Image Size 825X620 (micron).

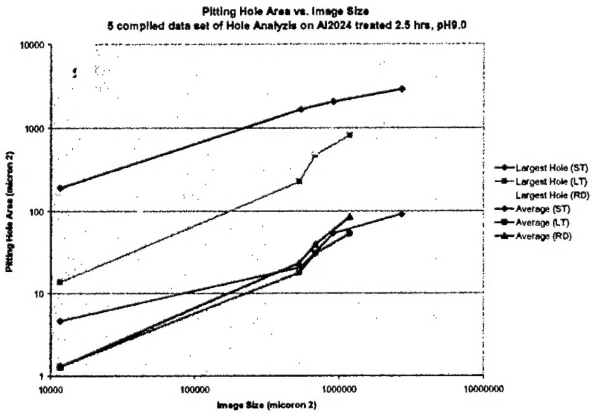
Pitting Hole Area vs. Image Size
5 compiled data set of Hole Analyzis on Al2024 treated 2.5 hrs, pH9.0
Pitting Hole Area (micron 2)
10000
1000
100
10
1
10000
100000
1000000
10000000
Image Size (micron 2)
Largest Hole (ST)
Largest Hole (LT)
Largest Hole (RD)
Average (ST)
Average (LT)
Average (RD)

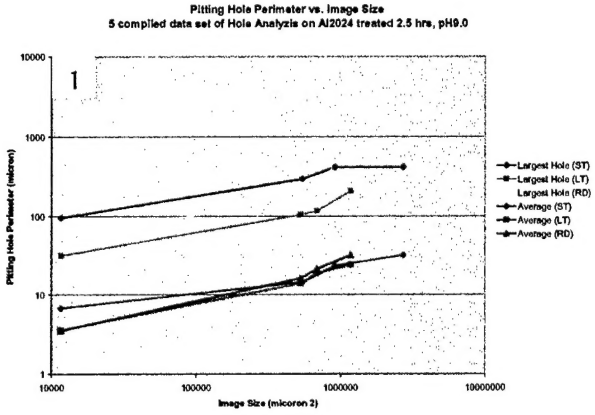
Pitting Hole Perimeter vs. Image Size
5 compiled data set of Hole Analyzis on Al2024 treated 2.5 hrs, pH9.0
Pitting Hole Perimeter (micron)
10000
1000
100
10
1
10000
100000
1000000
10000000
Image Size (micron 2)
Largest Hole (ST)
Largest Hole (LT)
Largest Hole (RD)
Average (ST)
Average (LT)
Average (RD)

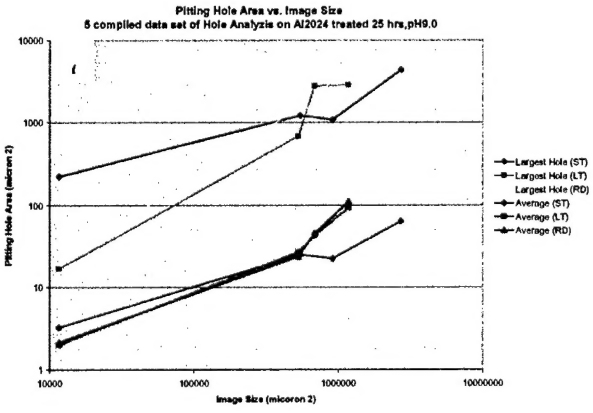
Pitting Hole Area vs. Image Size
5 compiled data set of Hole Analyzis on Al2024 treated 25 hrs,pH9.0
Pitting Hole Area (micron 2)
10000
1000
100
10
1
10000
100000
1000000
10000000
Image Size (micron 2)
Largest Hole (ST)
Largest Hole (LT)
Largest Hole (RD)
Average (ST)
Average (LT)
Average (RD)

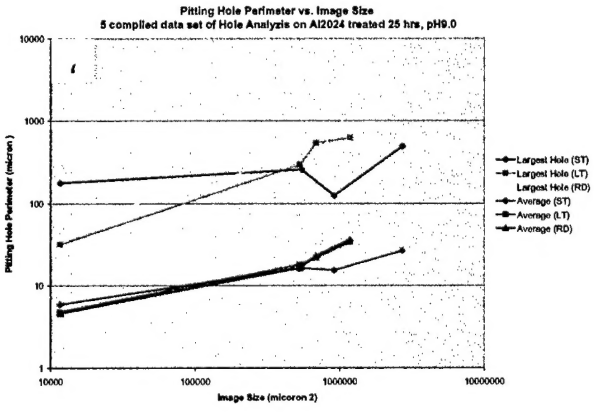
Pitting Hole Perimeter vs. Image Size
5 compiled data set of Hole Analyzis on Al2024 treated 25 hrs, pH9.0
Pitting Hole Perimeter (micron)
10000
1000
100
10
1
10000
100000
1000000
10000000
Image Size (micron 2)
Largest Hole (ST)
Largest Hole (LT)
Largest Hole (RD)
Average (ST)
Average (LT)
Average (RD)

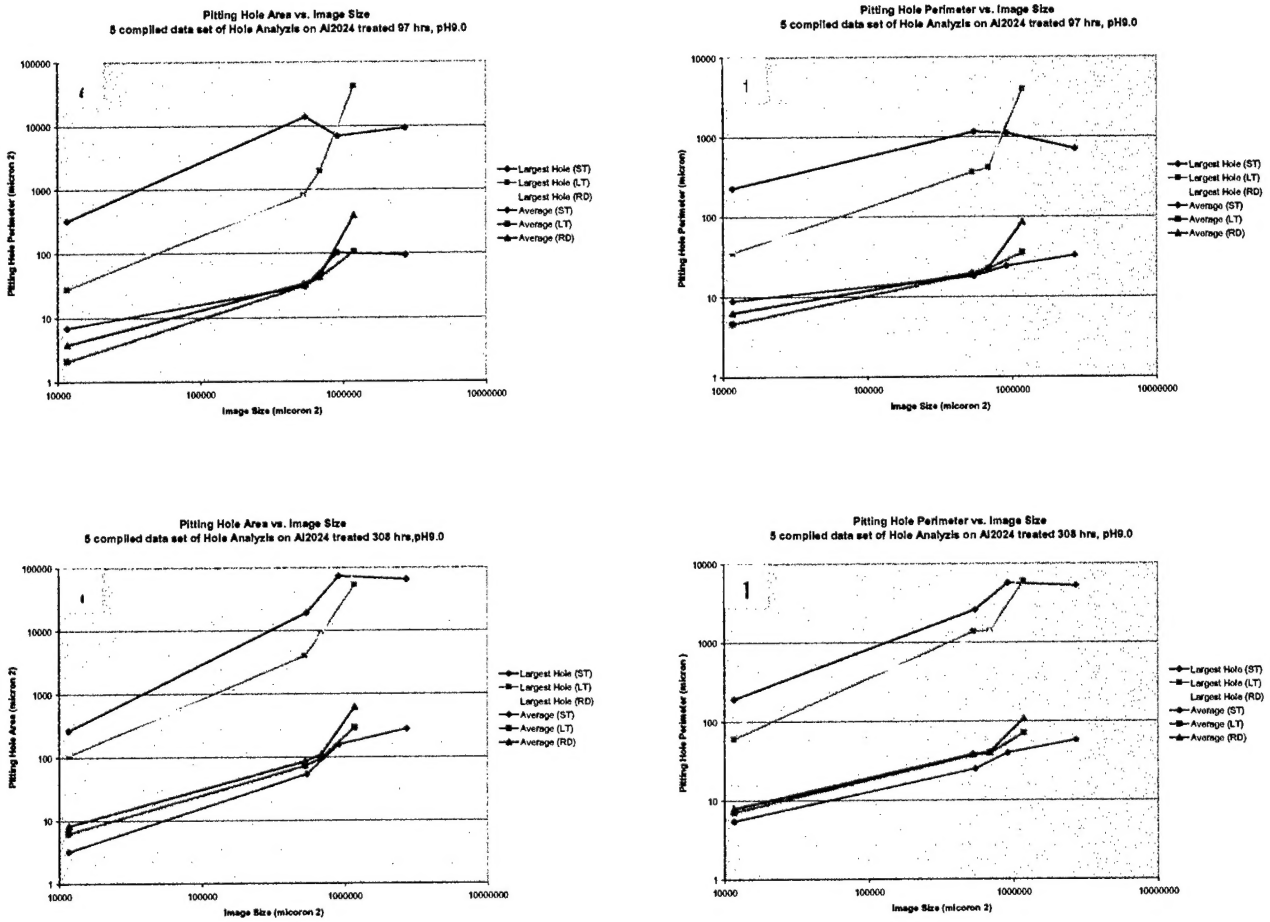

Fig.6. The area and perimeter of pits vs. image size for treating time 2.5 hrs (a, b), 25 hrs (c, d), 97 hrs (e, f) and 308 hrs (g, h).

Summary of results

1. At the beginning, the area of pitting holes slightly increase with time. After a certain time (ca. 25 ~97 hrs), the growth rate is sharp enhanced and at least logarithmic proportional to the treating time, as shown in Fig.2.
2. The RD surface is more reactive than the LT surface, while both of them are easier to be corroded than the ST surface. For a long treating time, for example 308 hrs, the RD and LT surfaces are almost totally damaged by the pitting corrosion, but the ST surface is much less corroded than the other two as shown in Fig.3. This phenomenon indicates that the RD and LT surfaces run a more important role in Multiple Site Damage (MSD) in airframe aluminum alloys than ST face.
3. The pitting holes grow independently at the beginning and joint each other when they meet, as shown in Fig. 3b. Most of the pitting holes show disk shape before merging. This can explain the similar shape of the largest and average curve between pitting hole area and perimeter, showing in Fig.4.
4. The parameters of pitting hole also increase with the image size in a approximately logarithmic pattern, indicating in Fig.4.
5. When the treating time is long, there are tons of tiny pits on the sample surface which can not be observed in detail even by SEM. As shown in Fig.3b, the cloudy parts within existed pitting holes are these micro pits. This phenomenon indicates these surfaces are already corroded even though these tiny pits can not be counted in our data. They are believed to be metastable pits and enhance the later corrosion.
6. The edge is more active than the center of the surface, showing in Fig 5.